Subsonic Interference Characteristics of Single and Twin Jet Afterbodies

E. H. Miller* and D. Migdal*
Grumman Aerospace Corporation, Bethpage, N. Y.

A model test program was conducted at 0.8 Mach number to examine important parameters in aircraft aft fuselage design. Thirteen twin jet interfairings were used to determine effects of interfairing length, interfairing base area, and engine spacing (combined with changes in maximum area and forebody shape). Three single jet configurations provided the effects of boattailing and served as a baseline for the twin jet tests. All configurations used a convergent (iris type) nozzle operating at a pressure ratio of 3.0. Test results show an optimum subsonic twin jet interfairing to be one that ends near the nozzle exit with zero base area. Small amounts of base area (3-8% of the maximum area) completely offset the favorable effects of interference between the exhaust jet and the freestream. Although geometrical changes that go along with increased engine spacing (larger maximum area, wider interfairing and flared forebody) tend to increase total drag, the effects on interference were small. Favorable interference levels, better than those of an equivalent pod, were obtained for all twin jet spacing ratios tested (S/D_{ENG} = 1.17, 1.43, and 2.37). It appears that the effects of increased spacing alone might be beneficial to afterbody performance.

Nomenclature

A_{BASE} = interfairing base area, in.^{2}
A_{ENG} = engine area at nozzle interface, in.^{2}
A_{JET} = jet exit area, in.^{2}
A_{MAX} = maximum afterbody area, in.^{2}
C_P = pressure coefficient, dimensionless
D_{ENG} = engine diameter at nozzle interface, in.
D_{INT} = interference drag, lb
D_N = nozzle drag, lb
D_{REF} = reference drag (jet off, nozzle removed, and corrected for engine cavity base pressure), lb
D_T = total aft end drag (including nozzle), lb
ΔD = change in fuselage drag from reference level, lb
ΔD_J = jet interaction parameter, lb
ΔF = effect of external flow on nozzle internal thrust, lb
L_T = total model length (fuselage plus nozzle), in.
M_0 = freestream Mach number
NPR = nozzle pressure ratio (nozzle total/ambient static)
P_{AMB} = ambient pressure, psi
q_0 = freestream dynamic pressure, psi
S = distance between nozzle centerlines, in.
X = interfairing length or distance from beginning of afterbody, in.
θ = interfairing half angle

Subscript

j = jet on
nj = jet off

Introduction

A LARGE portion of the drag of a modern tactical aircraft is attributable to the aft end.[1-3] It has been pointed out[2] that the design of afterbody fuselage and nozzle together with their associated aerodynamic interferences are of more critical importance than the aircraft forebody. The designer has always been plagued with the question of how much structure (interfairing) should be placed between the engines of a twin jet fighter. He also desired to know what, if any, performance changes were associated with different engine spacings. Separate optimization of nozzle thrust or aircraft drag is not adequate.[4] As learned from previous aircraft programs, testing the nozzle and fuselage separately does not reveal the interference effects which can be large. In order to maximize over-all performance, the exhaust nozzle/airframe interference must be understood and properly accounted for. This requires that back end configurations be tested with the nozzle installed, as well as separate reference drag and thrust tests,[4] thus, providing the necessary parameters to calculate the interference. Presently, there is a lack of suitable analytical techniques treating three dimensional configurations. This together with the absence of experimental data for important design parameters (most of the previously published data were for specific configurations) led to the present test program.

Performance of several afterbody configurations were studied by using force, and pressure instrumentation to determine thrust, drag, and interference. Thirteen twin jet configurations provided the effects of interfairing shape, size, and location, plus the related effects of nozzle spacing (the distance between engines). Three single jet models provided effects of afterbody shape and exhaust exit area for the case of an isolated pod. Convergent nozzles with smooth internal and external lines (simulating the iris type) were used on all twin and single jet configurations. The tests were run at 0.8 Mach number, and the data are presented for a nozzle pressure ratio of 3.0, which is typical of an installed turbofan operating at that speed. Three additional tests were conducted for each configuration (jet-off drag with the nozzle, drag without the nozzle, and nozzle static thrust) to establish baseline data for interference effects.

Model Description

Table 1 lists the geometrical data for the thirteen twin jet and three single jet configurations. The interfairings, in numerical order from left to right, are shown in Fig. 1.

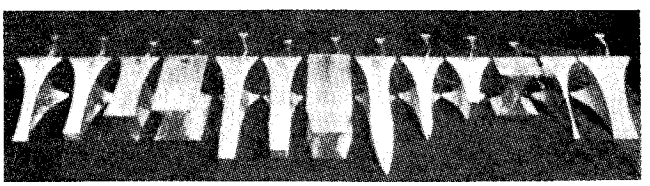

Fig. 1 Twin jet interfairings.

Received June 16, 1969; revision received October 10, 1969.
* Propulsion Project Engineer. Member AIAA.

Table 1 Model configuration data

Twin-Jet

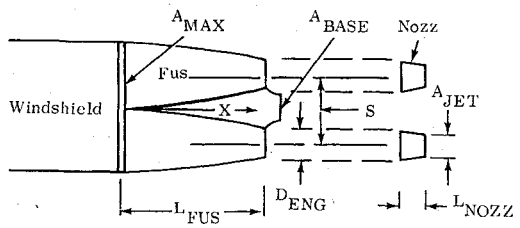

$\frac{L_{FUS}}{L_T} = 0.75$ $\frac{L_{FUS}}{D_{ENG}} = 3.14$

$\frac{L_{NOZZ}}{D_{ENG}} = 1.05$ $\frac{A_{ENG}}{A_{JET}} = 4.16$

$L_T = L_{FUS} + L_{NOZZ} = 7.30 + 2.43$

Config	X/L_T	(θ)	A_{BASE}/A_{MAX}	S/D_{ENG}	A_{MAX}/A_{ENG}
F-1	0.750	13°56'	0.000	1.43	2.32
F-2	0.750	10°55'	0.037		
F-3	0.750	5°22'	0.134		
F-4	0.750	7°46'	0.176		
F-5	1.000	10°7'	0.000		
F-6	1.000	7°59'	0.037		
F-7	1.000	3°54'	0.134		
F-8	1.240	7°59'	0.000		
F-9	0.750	13°56'	0.000		
F-10	0.428	13°56'	0.037		
F-11	0.298	3°54'	0.134	1.43	2.32
F-12	0.750	13°56'	0.000	1.17	2.09
F-13	0.750	13°56'	0.000	1.69	2.56

Single Jet

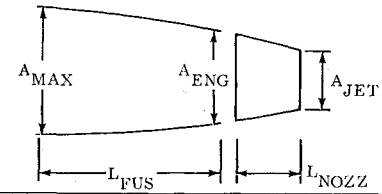

Config	A_{MAX}/A_{ENG}	A_{ENG}/A_{JET}	L_{FUS}	L_{NOZZ}
A	2.37	4.16	11.0	3.419
B	1.38	4.16	11.0	4.465
C	1.00	4.16	11.0	5.244

All except F-4 and F-11 had straight flat surfaces, both top and bottom. These two were contoured near the aft end to keep within the afterbody lines. Interfairing half angle (θ in Table 1) is measured in the vertical plane at the aft end.

Twin jet models (Fig. 2) were constructed in modular fashion, the left fuselage being separable from the right. Interfairings were individually added on to the basic twin fuselage. The body contained eight pressure taps; the nozzle had six. Four pressure taps were located along the interfairings.

The single jet tests were run with three models (Fig. 3). They all had a maximum diameter of 5 in. and a fuselage length of 11 in. The nozzles were geometrically similar and all had the same ratio of A_{ENG}/A_{JET} (4.16). The parameter varied was A_{MAX}/A_{ENG} (1.00, 1.38, and 2.37 as noted in Table 1).

Testing was performed in the Fluidyne Corporation 22-in. × 22-in. transonic wind tunnel. The models were mounted to a cantilevered sting which also supplied the nozzle air. In the twin jet assembly (Fig. 4) the flow is split from one circular pipe to mate with the 2 nozzles. The windshield transition piece changes the external sting contour from a circular cross section to an elliptical one just upstream of the model. External forces on the model were measured downstream of the metric station. The single jet model installation used the conventional circular pipe without the transition piece.

Direct force measurements were taken with a strain gage type balance to provide thrust coefficients. Digital force readings were recorded on tape and electrically marked for a given test point. Pressure data, to gain insight into the

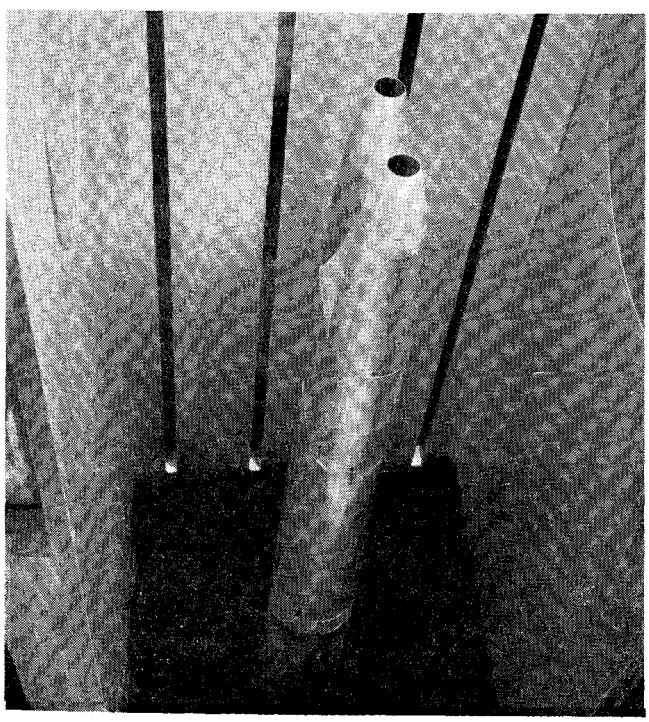

Fig. 2 Typical twin jet model.

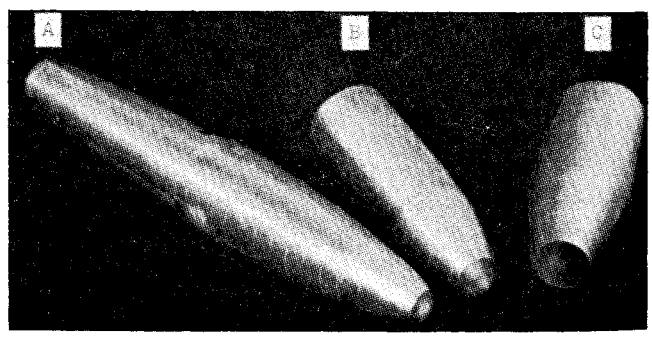

Fig. 3 Single jet models.

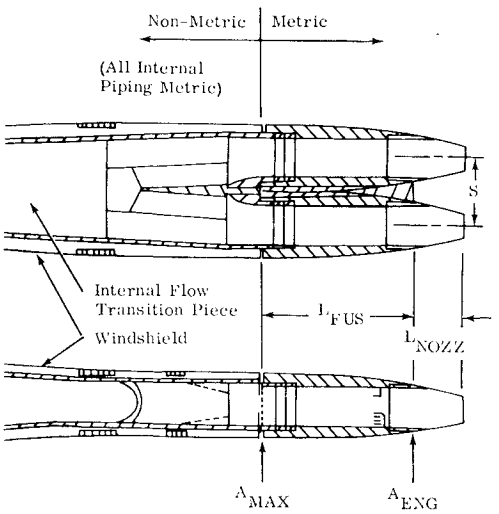

Fig. 4 Twin jet model assembly.

afterbody flowfield phenomena, were also recorded. Readings were made by photographing mercury manometer boards. Eighteen pressure readings were recorded for a typical twin jet configuration.

Effects of Interfairing Design

Results from the eleven interfairing configurations tested at constant spacing ratio (1.43) are presented in Figs. 5–9 using parameters derived from force balance data. Each is plotted as a function of base area with curves faired in to represent interfairing length.

Figure 5 shows basic reference drag levels of the twin jet body and interfairing without the nozzle installed. The drag levels increase rapidly as the interfairing is terminated upstream beyond the basic body length ($X/L_T \leq 0.75$). Although an optimum interfairing base area appears to exist, the effect is not large.

Total aft end drag (which includes nozzle drag) is shown in Fig. 6 for the jet-off case and for jet on in Fig. 7. Neither case shows an optimum base area to exist. And for interfairings that terminate near the nozzle exit ($X/L_T = 0.75$–1.24) there is no noticeable effect of length on the total drag. Note that in this length range, the slope of the drag increase with base area is greater for the jet-on case (Fig. 7) than with the jet off (Fig. 6). Also, the jet-on drag is lower than jet off

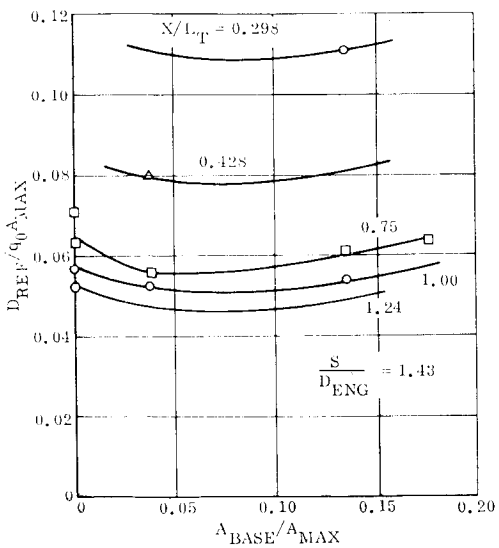

Fig. 5 Twin jet reference drag.

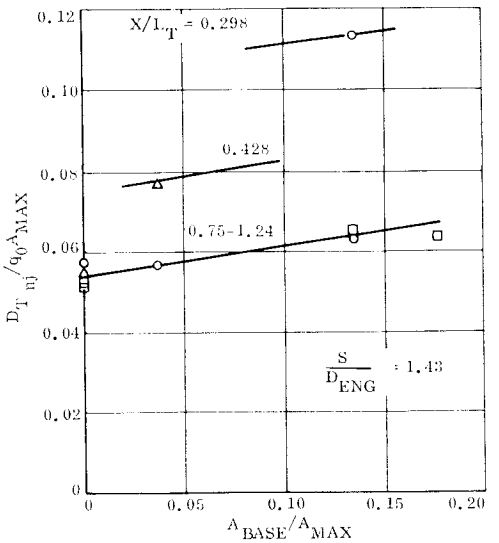

Fig. 6 Twin jet total aft end drag, jet off.

at zero base area. This is because at the jet operating condition ($NPR = 3$) there is a favorable interaction between the expanding jet and the external flow over a smooth body with no base. But when the base becomes large enough, the jet can aspirate the area, making base drag increase to levels higher than with no jet. The net effect is that favorable interactions on the outboard side of the nozzle are offset by a drag increase on the inboard sides and base, as base area reaches a certain value. This value is about 12% of maximum area for the twin jet configuration tested as illustrated by the jet interaction parameter $\Delta D_j = D_{Tj} - D_{Tnj}$ in Fig. 8.

Interference drag, a parameter developed at Grumman[4] for comparing various fuselage/nozzle configurations, is shown in Fig. 9. This parameter normally contains three terms: $D_{INT} = \Delta F + D_{Nj} + \Delta D$. For these tests, ΔF (nozzle internal thrust loss due to external flow) is zero because the nozzle was convergent and was operated with choked flow ($NPR = 3$). Figure 9 therefore contains external nozzle drag with the jet on (D_{Nj}) plus the change in drag on the body and the interfairing (ΔD) because of jet effects and the presence of an iris type convergent nozzle. Negative values of D_{INT} are favorable and indicate either that thrust (negative drag) is acting on the external nozzle surfaces or that a large reduction in body and interfairing drag has been achieved. As shown in Fig. 9, favorable interference occurred with all interfairing lengths when no base area was present. Beyond a small amount of base area (3–8%) adverse interference occurred with all except the shortest interfairing.

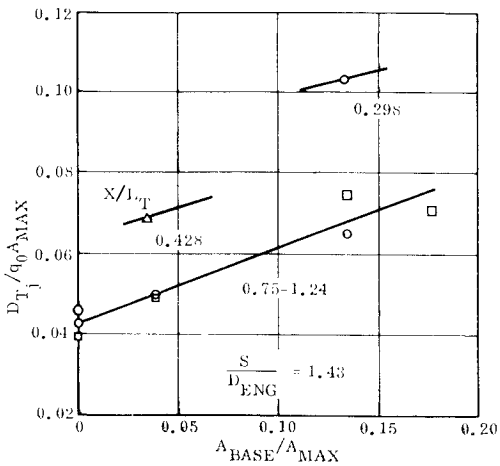

Fig. 7 Twin jet total aft end drag, jet on.

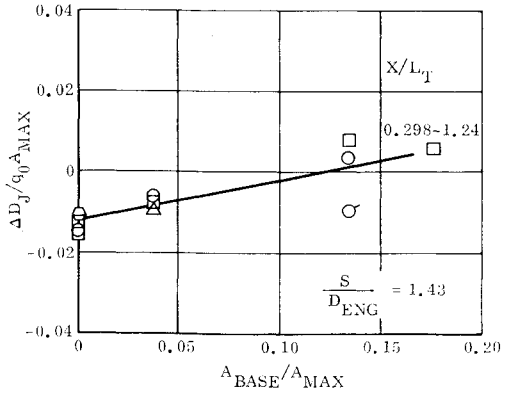

Fig. 8 Twin jet interaction parameter.

Interfairing Base Region

Base pressures measured at the end of the twin jet interfairing exhibited typical trends. Representative data are presented in Fig. 10 for four interfairings of the same length but with a systematic variation in half angle and base size. Note that the jet effect (NPR = 3 vs jet off) tends to aspirate larger bases (F-3 and F-4) and helps pressurize smaller bases (F-1 and F-2). Positive base pressures (thrust) occurred at angles above 10° because external flow over the top and bottom surfaces was turned enough to interact within the base region. However, it should be recognized that only a small amount of base thrust existed (Fig. 11) because when positive pressures were achieved, the base areas were quite small in size.

Single Jet Afterbodies

Three isolated body shapes were tested with geometrically similar nozzles (A_{ENG}/A_{JET} const). All data are presented in Fig. 12 to illustrate the relationships between the various drags and parameters involved.

Although the data exhibit common trends, it is important to note the magnitude of the effects. Basic body drag (D_{REF}) increases rapidly as boattailing (pressure drag) is added beyond that of a cylinder (friction drag only). But with axisymmetric boattails there is an aft recompression which drastically reduces nozzle drag (D_{Nnj}). Such recompression makes the total jet-off drag (D_{Tnj}) decrease with boattailing in a typical fashion. Operation of the jet produces a favorable interaction which lowers total drag (D_{Tj}) levels by the amount ΔD_j. The jet interaction (ΔD_j) occurred in this case (isolated body) mostly on the nozzle. Therefore, the interference drag (D_{INT}) can be considered equal to the jet-on nozzle drag (D_{Nj}) in Fig. 12. Since favorable interference occurred with boattailing beyond A_{MAX}/A_{ENG} of about 1.6, net external forces on the nozzle were in the thrust direction in this range.

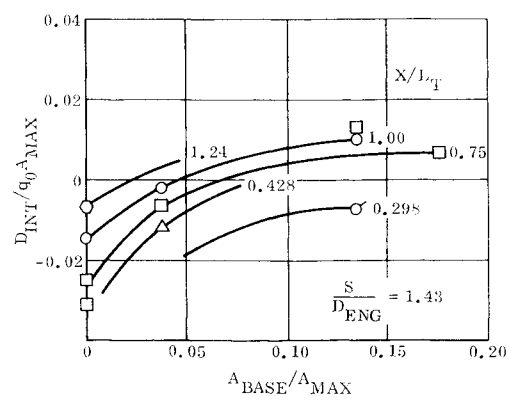

Fig. 9 Twin jet interference drag.

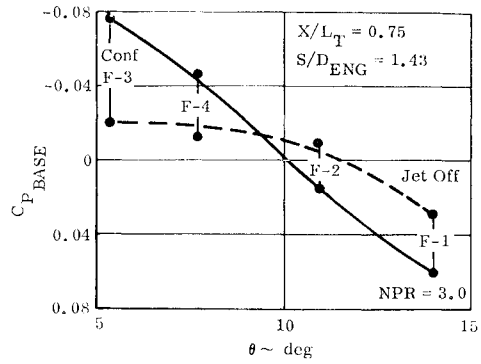

Fig. 10 Twin jet interfairing base pressure.

Twin Jet Spacing and Related Effects

A parameter of interest in afterbody design is the spacing between engines in a twin jet fuselage installation. However, as the distance between engines is changed, other geometrical changes must take place in a practical fuselage which tend to mask the pure effect of spacing. In this test program, three fuselage configurations describe the combined effects of changes in spacing ratio (S/D_{ENG}), maximum cross-sectional area (A_{MAX}), and forebody shape (windshield) as illustrated in Fig. 13.

The three twin jet fuselage shapes (F-1, F-12, and F-13) represent a systematic variation of geometry when the area between two round nacelles is completely filled by an interfairing. Each nacelle had a maximum to engine area ratio of 2.045 and the round nacelles just touched at a spacing ratio of 1.43 (configuration F-1). Smaller spacings (as for F-12) were achieved by removing a portion of the nacelle inboard surface. Although the straight line relationship in Fig. 13 extends down to a single jet cylindrical pod (configuration C), practical considerations such as "flat sided engines" rule out spacing ratios between 1 and 0.

Also note in Fig. 13 that the windshield was made more divergent as spacing was increased. This represents a flared forebody and produces lower than ambient static pressures at the windshield/afterbody interface for the wider spacings.

Therefore, data from these test configurations should not be plotted vs S/D_{ENG} and viewed as the pure effect of spacing alone. However, test results can be compared with a single jet equivalent pod of the same A_{MAX}/A_{ENG} (illustrated in Fig. 13). Such a comparison is made for total aft end drag (D_{Tj}) in Fig. 14 where the vertical distance between single and twin jet curves is the drag increase from an equivalent pod. The drags are equal at an A_{MAX}/A_{ENG} of 1.97 which in this test corresponds to the minimum practical spacing (S/D_{ENG} = 1 for engines that just touch each other).

Beyond an A_{MAX}/A_{ENG} of 1.97, drag levels of the twin jet increased because of forebody effects (interface pressures at the nozzle metric station are less than ambient with flared wind-

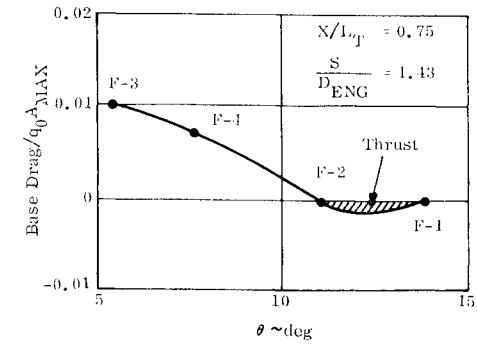

Fig. 11 Twin jet base force.

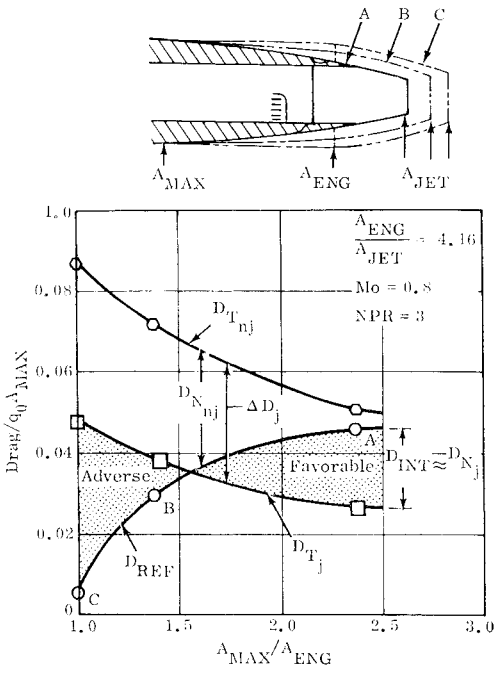

Fig. 12 Single jet test data.

shield), extra surface area of the wider interfairing, and blockage of external flow by the greater cross-sectional area. But, note (Fig. 14) that the twin jet drag is not as high as the single jet cylindrical pod.

Favorable twin jet interference levels (negative values) resulted and were twice as good as those of the single equivalent pod (Fig. 15). This resulted from either a large reduction in pressure drag on the afterbody (nacelles and interfairing), or positive pressures on the nozzle external surfaces (thrust), or both. It is estimated that about half of the favorable interference occurred on or near the interfairing because the twin jet level is about double that for a single equivalent pod.

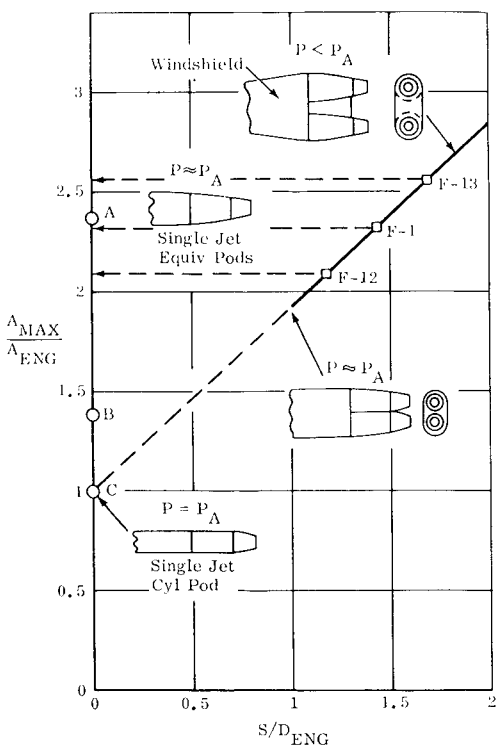

Fig. 13 Twin jet geometrical relationships.

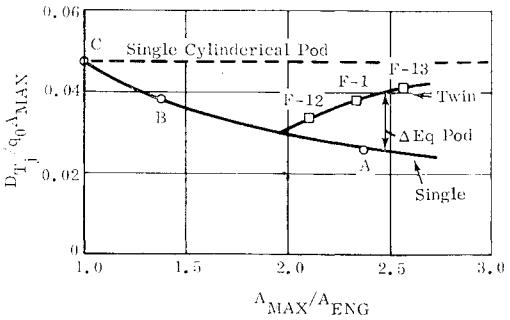

Fig. 14 Single and twin jet drag.

Also note in Fig. 15 that twin jet interference improved as spacing ratio was increased from 1.17 (F-12) to 1.69 (F-13) even though the wider spaced configuration (F-13) had more drag (Fig. 14). This trend indicates that if spacing were increased without increasing drag, the favorable effect on interference might be even more pronounced.

Conclusions

Model data, describing the drag and interference characteristics of several afterbody configurations, indicate that subsonic (0.8 Mach numbers) performance levels are sensitive to many parameters. Twin jet test results at a spacing ratio of 1.43 are 1) short interfairings produced high drag levels with any base area, 2) interfairings terminating at or near the nozzle exit reduced drag by about $\frac{1}{3}$, 3) zero base area produced the best performance at any interfairing length, 4) favorable jet interactions on the nozzle were offset by base drag when the base area exceeded 12% of maximum cross-sectional area, 5) favorable interference (i.e., total body and nozzle drag less than body drag without nozzle) occurred for all configurations with zero base area and became adverse beyond base areas of 3–8% for most interfairings, and 6) while positive base pressures occurred with interfairings having base areas less than 5% and angles above 10°, the base "thrust" force was quite small.

The combined effects of increasing spacing ratio, interfairing width, maximum cross-sectional area, and forebody flare were 1) an increase in twin jet drag to levels higher than an equivalent single jet pod, but lower than a pure cylindrical pod, 2) a slight increase in favorable interference, from levels that were twice as good as an equivalent pod, and 3) an indication that the effects of increased spacing alone may be beneficial for twin jet performance, since the other

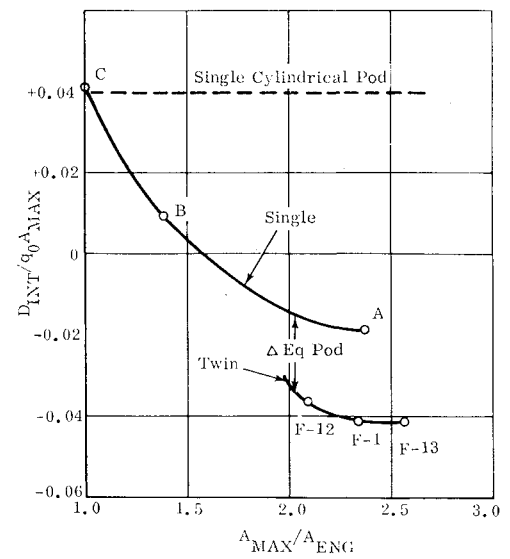

Fig. 15 Single and twin jet interference.

geometrical changes tend to decrease performance. Single jet results show that upstream boattailing can reduce the drag of a cylindrical pod by 50% or more due to favorable interference.

References

[1] Greathouse, W. K., "Blending Propulsion with Aircraft," *Space Aeronautics*, Vol. 50, No. 2, Nov. 1968, pp. 59–68.

[2] Nichols, M. R., "Aerodynamics of Airframe—Engine Integration of Supersonic Aircraft," TN D-3390, Aug. 1966, NASA.

[3] Corson, B. W., Jr. and Schmeer, J. W., "Summary of Research on Jet Exit Installation," TMX-1273, 1966, NASA.

[4] Migdal, D. and Greathouse, W. K., "Optimizing Exhaust/Nozzle Airframe Thrust Minus Drag," Paper 680294, May 1968, Society of Automotive Engineers.

MAY-JUNE 1970 J. AIRCRAFT VOL. 7, NO. 3

Approximate Analysis of a Flat, Circular Parachute in Steady Descent

EDWARD W. ROSS JR.
U.S. Army Natick Laboratories, Natick, Mass.

A theory is presented for the stress analysis of a flat, circular parachute in steady, vertical descent. Unlike previous treatments of the problem, this theory does not assume that the shape is known. Instead, the theory derives relations between the pressure distribution in the opened condition and the shape, drag and stresses in lines and fabric. The theory results in a nonlinear third order system of ordinary differential equations with boundary conditions at both vent and skirt. This system was solved by a computer program based on the Runge-Kutta method of numerical integration. The results are in fairly good agreement with measurements on parachutes. The computer program can be used for studies of effects of design changes on shape, drag and stress, and the results of a small study of this sort are included.

Nomenclature

A_0, A_1, A_2, A_3 = constants in canopy pressure distribution
C_{D0} = drag coefficient based on flat circular area
C_p = coefficient of net pressure
C_c, C_f = stress coefficients in cords, fabric
D = drag of canopy
D_p, D_0 = diameters in opened and flat circular states
E_c, E_f, E_L = elastic moduli of cords, fabric, load lines
f = $1 + (N_c/E_c)$
G = number of gores
J = dimensionless load line length
L_0, L = length of load lines in undeformed and deformed states
N_c, N_f = tension force in cords, fabric
N_θ, N_n = force resultants on cords in circumferential and normal directions
n_s, n_f = dimensionless force in cord, fabric
n_c = dimensionless circumferential force resultant on cords
p = net outward pressure on gore fabric
q = dimensionless pressure
R = radius of particle in flat circular state
R_i, R_0 = vent and skirt radii in flat circular state
r = radius of cord in opened state
r_{AB} = circumferential radius of curvature of gore
s = arc length of cord
U_f, U_L = dimensionless elastic constants
V = vertical velocity
W = dimensionless drag
x = dimensionless radius in flat, circular state
x_0 = dimensionless skirt radius in flat circular state
y = dimensionless radius in opened state
Z, Z_0 = axial cylindrical coordinate of cords and gore centerline
z, z_0 = dimensionless axial coordinate of cords and gore centerline
α = included angle of gore
β = edge angle of gore bulge
$\gamma_s, \gamma_f, \gamma_L$ = strains in cord, fabric, and load lines
δ = depth of bulge
Δ = dimensionless depth of bulge
θ = angle between load line and axis
Λ = load line length ratio = $L_0/D_0 = JR_i/(2R_0)$
ρ = mass density of air
σ' = contact length between adjacent gores
σ = dimensionless contact length between adjacent gores
τ = dimensionless function measuring contact of adjacent gores
ϕ = angle between cord direction and horizontal

Received February 7, 1969; revision received October 6, 1969. The author is indebted to the members of the Research and Advanced Projects Division in the Airdrop Engineering Laboratory at the U.S. Army Natick Laboratories, particularly E. J. Giebutowski, for both help and instruction during the course of this work.

* Staff Mathematician.

1. Introduction

IN recent years repeated attempts have been made to analyze the behavior of parachutes and devise formulas suitable for their design. Much progress has been made, but the state of knowledge is still not wholly satisfactory. The best analyses currently available, Heinrich and Jamison[1] and Topping, Marketos, and Costakos[2] rely on knowing the deformed shape as well as the pressure distribution before the stresses are analyzed even in steady descent. Present knowledge about large deflections of structures suggests that it should be possible to calculate the stresses and deformed shape concurrently, although some assumptions must still be made about the pressure distribution in the deformed state. We shall undertake to do this in the present paper.

To be specific, we shall analyze a flat, circular canopy in steady, vertical descent by using the ideas of large-deforma-